

Vertical structure and variability of currents on the southern Brazilian inner shelf at 32°S

Julia Gil dos Santos¹ , Carlos Alberto Eiras Garcia^{1,2,*} 

¹ Universidade Federal do Rio Grande (FURG). Avenida Itália Carreiros, Km8, Rio Grande - RS, 96203-900, Brazil.

² Universidade Federal de Santa Catarina (UFSC). R. Eng. Agrônomo Andrei Cristian Ferreira, s/n - Trindade, Florianópolis - SC, 88040-900, Brazil.

* Corresponding author: garcia.io.furg@gmail.com

ABSTRACT

This study investigates the impact of winds, tides, and river discharges on the coastal current and salinity variability of Southern Brazil's inner shelf. Data on wind speed, current, surface salinity, and temperature were collected for analysis from a metocean buoy of the Brazilian Coastal Monitoring System (SiMCosta). The observed current time series can be interpreted as a sum of highly variable flows correlated with local wind stress, and a residual mean current flowing southward along the coast at a few centimeters per second. Tidal currents were predominantly diurnal, albeit negligible, representing approximately 1.7% of the current variance in the region. We observed a prevalence of northwest winds and southeastward currents on the inner shelf, as well as an intermittent flow in both the alongshore and cross-shore directions due to meteorological frontal system passages. The power spectrum of both current components presented similar frequency patterns, indicating the prevalence of high-energy events in periods of 3 to 10 days over the entire time series. The alongshore current is highly correlated ($r=0.73$, $p<0.05$) with alongshore wind and a delay of 3 hours. In the low- (period >40 h) and high-frequency (period <40 h), the temporal lags were of 5 and 3 hours, respectively, with correlations of 0.79 ($p<0.05$) and 0.60 ($p<0.05$). The wavelet analysis has shown that high-energy events in alongshore wind stress are more common between August and October and less often between February and March, with similar surface currents and salinity patterns. A decrease in surface salinity during the winter season was observed due to the high level of Patos Lagoon's outflow. Mean daily salinity correlated negatively with Patos Lagoon's outflow, however part of this variability is associated with the intrusion of Patos Lagoon's plume and the passage of frontal systems.

Keywords: Coastal circulation; direct current measurements; tidal currents; south Brazilian inner shelf

INTRODUCTION

The continental shelf can be defined, in geological terms, as the part of the continent that is submerged into the ocean. It is usually subdivided as internal platform and external platform, geologically separated by the isobath

of 50 m (Mendes, 1984). The inner shelf can be understood as the "nearshore region" (Mitchum and Clarke, 1986). According to Lentz (1995), the inner shelf plays a key role in the overall shelf dynamics because it is the region where the circulation adjusts to the coastal boundary conditions.

The main forcing mechanisms that generate and act over water transport dynamics are tides, winds, impact of freshwater discharge, Coriolis effect, and local bathymetry. The time scale of these processes ranges from semidiurnal (12 h)

Submitted: 20-May-2022

Approved: 12-Apr-2023

Associate Editor: Ronald Souza



© 2023 The authors. This is an open access article distributed under the terms of the Creative Commons license.

to interannual and they can be deterministic processes (i.e., tidal) or not (i.e., year-to-year variations in wind or river discharge rates). Regarding wind forcing, the time scale variation changes with the geographical area, and the synoptic scale associated with the passage of frontal systems can dominate some regions (Castro and Lee, 1995; Castro et al., 2006).

An important impact on the circulation of shelf waters happens when freshwater derived from a hydrographical basin encounters ocean waters. According to McClimans (1988), the seaward expansion of low salinity waters is usually called a river plume, which is limited by a front showing differences in water color and the formation of a foam line (Garvine, 1984; Mann and Lazier, 2005). The presence of this feature may change circulation patterns due to differences between water properties, causing variation on its physical parameters. This variation is largely due to the differences in salinity. In theory, a coastal river discharging freshwater into a saline environment forms an anomaly in both volume and density, resulting in a characteristic circulation pattern (Soares et al., 2007); freshwater tends to flow and stay at the surface while ocean water remains at the bottom, which promotes a density gradient along the water profile.

Although dependent on inlet conditions, studies have demonstrated an opposite behavior in the spread of coastal plumes, with low salinity waters flowing in close contact with the bottom of the ocean (Beardsley and Hart, 1978; Ikeda, 1984; Chao and Boicourt, 1986; Chao, 1988a, 1988b; Yankovsky and Chapman, 1997; Garvine, 1999). This different circulation pattern is normally associated with plumes that have large extensions, while surface plumes are often associated with smaller discharges. Hence, a large volume of freshwater discharge can cause freshwater accumulation close to the estuary's mouth, which may occupy the entire water column, and make freshwater flow close to the ocean floor. Changes in the pressure gradient may induce changes in the plume orientation, which will be influenced by coastal current circulation nearshore. Moreover, tidal currents were reported as an important force in the propagation of plumes at the bottom (Kirincich

and Hebert, 2005; Guo and Valle-Levinson, 2007). Salinity variations, however, could be associated to the river plume, especially at the surface. Regarding mixing process, McClimans (1988) indicates that an important engineering aspect of river plumes is the initial dilution or mixing with seawater, or brackish water, within the estuarine system. Once the plume is formed, its seaward dynamics and behavior will depend on the inner shelf's local current circulation.

The resulting flows over the inner shelf, or coastal currents, have a huge impact on the coastal area. They can be structured flows or not, stemming from the Earth's rotation, winds, and density differences. Problems caused by intense coastal currents associated with gravitation waves and rising sea levels can lead to erosion and flooding in coastal areas, destruction of seaside buildings, as well as siltation of ports and navigation channels (Costa and Möller, 2011). Therefore, the study of coastal currents, the determination of their variability and related processes are essential to coastal management and environmental issues.

The hydrodynamic of southern Brazil's inner continental shelf – around 32°S – has been studied and described in the past using hydrographic cruises (Möller et al., 2008; Piola et al., 2008) and modelling techniques (Palma et al., 2008; Matano et al., 2010; Mendonça et al., 2017). Most of the local circulation research in the coastal waters close to Patos Lagoon was made using numerical modeling (Marques et al., 2008; Marques et al., 2010) and just a few studies used direct *in situ* measurements of metocean data. Most of the studies with *in situ* data used a time series shorter than six months, hence, the seasonal characteristics were not analyzed.

With the implementation of the Brazilian Coastal Monitoring System (SIMCosta) – an integrated observational system aimed at continuous, automatic, and real-time monitoring of meteorological and oceanographic parameters for ecological and climatic studies – the time series analysis gained strength and became an important ally in the gathering of more information on the inner shelf coastal dynamics close to Patos Lagoon's mouth.

Thus, this paper aims to contribute to a better understanding of southern Brazil's inner shelf coastal current dynamics – based on a vertical current profile – close to Patos Lagoon's mouth, at approximately 32°S latitude. The study focuses on the structure and variability of coastal currents caused by forcing mechanisms, particularly tides, winds, and river discharges. The article is separated into five main topics: (1) description of winds, river discharge, and oceanographic properties; (2) current structure and variability; (3) analysis of tidal currents; (4) analysis of surface detided currents and its interaction with local wind and river discharge; and (5) salinity and current variability during winter cold front passages.

THE SOUTHERN BRAZILIAN SHELF AND THE PATOS LAGOON

The southern Brazilian shelf is narrow in the northern part (110 km) and widens up to 170 km in the south. The shelf break is located around the 180 m isobath. The inner shelf is dominated by coastal currents originated at Patagonia's coast (Piola and Rivas, 1997) and by the La Plata river discharge (Framiñan and Brown, 1996; Guerrero et al., 1997; Burrage et al., 2008). The outer shelf is influenced by the western boundary of the Brazil Current (Castro and Miranda, 1998), whereas the inner shelf receives freshwater contributions from La Plata river (depending on the season) and Patos Lagoon (Moller et al., 1996, 2001; Piola et al., 2005, 2008). The influence of the South Atlantic High-Pressure system, anticyclones of polar origin, and extratropical cyclones contributes to the high spatial variability of wind circulation at synoptic time scales over the southern continental shelf. The tides in the region are mixed with diurnal dominance and their effects are restricted to both the coastal zone and the estuarine region of the Patos Lagoon (Moller et al., 2001).

The southern Brazilian continental shelf (from 22°S to 34°S) is usually covered with waters involved in southward motion (except in the winter) due to: (1) northeasterly and easterly prevailing winds (except in the autumn

and winter); (2) the continental slope in the area being occupied with the southward flow of the Brazil Current and; and (3) according to water mass analysis studies (e.g. Miranda, 1972; Miranda and Castro, 1979), the region is covered mostly by water of tropical origin all year round, indicating the presence of southward advection (Zavialov et al., 2002). In addition, Pereira (1989) has predicted a dominance of southward flow which could only be overridden by sufficiently strong southern winds.

On the other hand, there is an unexpected presence of northward net transport over the shelf that sometimes can be traced as far north as 23°S (Campos et al., 1996; Stevenson et al., 1998; Zavialov et al., 1998; Piola et al., 1999). Zavialov et al. (2002) attribute this northward flow as the Rio Grande Current. Moreover, the region has the well-known entrance of a large amount of freshwater in the coastal zone from Rio de la Plata and from the Patos-Mirim Lagoons complex, which causes a strong impact concerning the shelf dynamics since it produces a lateral salinity gradient that induces a northward residual flow (Pereira, 1989; Zavialov et al., 1998) usually modulated by wind action.

Patos Lagoon is a shallow and long coastal lagoon (Figure 1), with nearly 275 km of extension. According to Marques (2005), the rivers Taquari and Jacuí (tributaries of the Guaíba river) along with the river Camaquã are the main tributaries of Patos Lagoon. Möller et al (2001) sustain that the rivers exhibit a typical mid-latitude flow pattern with high discharge in late winter and early spring, and low to moderate discharge expected during summer and autumn. The rivers also present large year-to-year discharge variations. Patos Lagoon is connected to the South Atlantic Ocean by a natural channel (modified by training walls) that is close to 1 km wide and 12 m deep (Moller et al., 2001). This artificial channel is Patos Lagoon's only runoff, with an annual mean discharge of approximately $2000 \text{ m}^3 \text{ s}^{-1}$, with seasonal fluctuations ranging from more than $8000 \text{ m}^3 \text{ s}^{-1}$ to less than $1000 \text{ m}^3 \text{ s}^{-1}$ in late austral winter and midsummer, respectively (Moller et al., 2001).

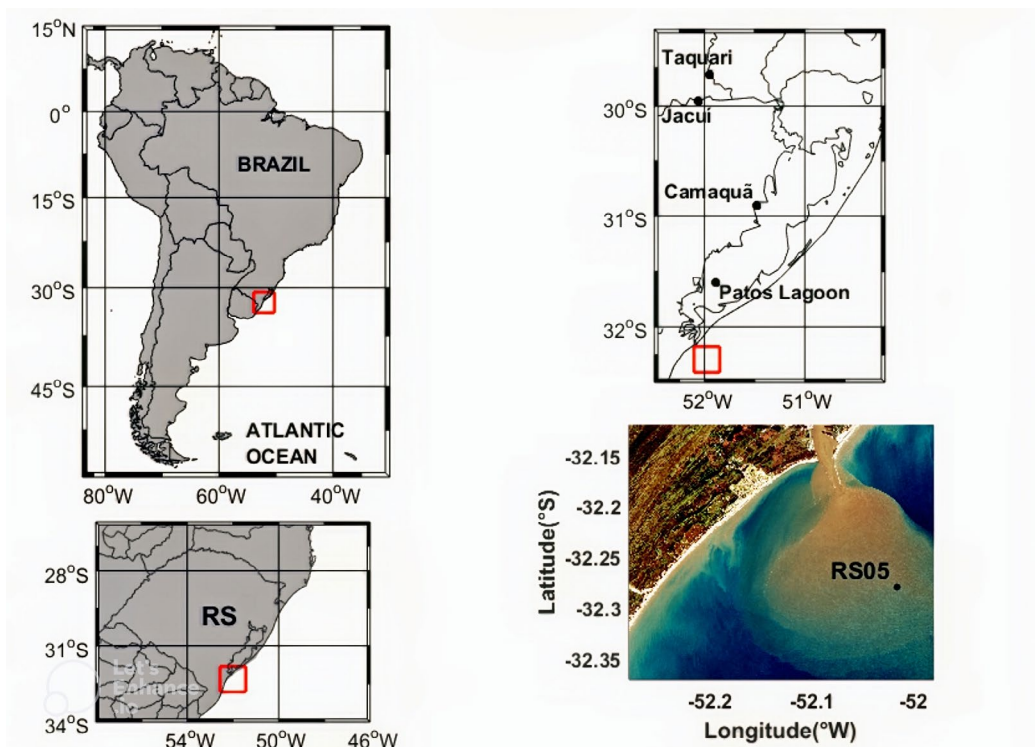


Figure 1. Study area. The Landsat 8 true color composition image, obtained on August 25, 2017, shows the location of the SiMCosta RS05 buoy, close to the mouth of Patos Lagoon. The plume is clearly seen due to its high content of suspended solids.

The main lagoon axis is northeast-southwest oriented and coincident with the dominant wind regime. Historical studies reported the lagoon responding to wind forcing (Malaval, 1922; Motta, 1969), in which NE winds contribute to seaward flow, whereas southerly winds, mainly the southwesterly, can produce the opposite effect. Therefore, NE winds are particularly important for the circulation and dynamics of the inner shelf (and buoy site), once they promote lagoon outflow. They are dominant throughout the year, although southerly winds become more important in autumn and winter when the frontal systems constrain coastal water landward more frequently.

Previous studies presented similar conclusions concerning wind as an important forcing mechanism on the coastal waters close to Patos Lagoon (Castelao and Moller Jr, 2006; Möller et al., 2008; Marques et al., 2010). Marques et al. (2009) used numerical modeling to investigate the influence of the main physical forcing factors acting on Patos Lagoon's coastal plume formation and behavior. The importance of

winds acting as the main mechanism controlling the behavior of Patos Lagoon's coastal plume in synoptic time scales was notable. The authors of the study concluded that winds of moderate intensity can mechanically reverse the plume orientation. They also concluded that the intensity of the river discharge flowing higher than $2000 \text{ m}^3 \text{ s}^{-1}$ contributes to the coastal plume formation. Marques et al. (2010) investigated the importance that straining and advection had on the inside of Patos Lagoon's coastal plume and concluded that northeasterly and northwesterly wind conditions – associated with southwestward and southeastward transportation of the plume – contributes to spreading the brackish waters offshore, increasing the vertical stratification of the coastal area. On the other hand, southeasterly and southwesterly wind conditions, associated with the northeastward transportation of the plume, contributes to the vertical mixing of the inner continental shelf. Near the Patos Lagoon's mouth, the occurrence of stratification/vertical mixing processes is associated with the lagoon

exchange, independently of the intensity of river discharge. The authors also concluded that the plume behaves as an hypopycnal plume covering the first meter of depth. Burrage et al. (2008) suggested the plume maintains its integrity over the southern Brazilian shelf as a relatively symmetric, ageostrophic, frictionally dominated plume with significant across-shelf, and modest along-shelf development.

STUDY AREA

The study area extends along the Rio Grande coastline defined by latitudes of about 31°54'S and 32°33'S and longitudes 52°16'W and 51°46'W (Figure 1). This area includes the Patos Lagoon plume that extends about 25 – 40 km offshore. Within the study area, at latitude 32°17'45.6"S and longitude 52°01'26.4"W, a metocean buoy named SiMCosta RS05 was moored at 20 m depth, approximately 14 km from the coast, and 8 km from Barra de Rio Grande (Figure 1). The SiMCosta RS05 buoy site receives the influence of Patos Lagoon's waters due to the proximity to the coastal lagoon channel (modified by training walls) (Figure 1).

DATA AND METHODS

This study is based on the analysis of time series of vertical currents, wind, surface salinity, and surface temperature, recorded at an hourly interval during 325 consecutive days by the following instruments on the SiMCosta RS05 buoy: Seabird SBE 37-SMP, a temperature and salinity/conductivity recorder; Nortek Aquadopp Z-Cell 600 kHz, an acoustic Doppler current profiler (ADCP); and Gill Instruments WindSonic, an ultrasonic anemometer. The hourly records span from December 06, 2016, to October 27, 2017. All the *in situ* salinities used the practical salinity scale, defined as a conductivity ratio with no units. The ADCP was programmed to measure currents in 25 bins along with the vertical profile with a cell size of 1 m. As the head of the ADCP is located 0.5 m from the free surface of the ocean, and there is a blank area of 0.5 m, the instrument measures currents from 1 m deep and below (i.e.: bin 1 measures currents from 1 to 2 m, at the depth of 1.5 m; bin 2 from 2 to 3 m, at the depth

of 2.5 m; and so on). Only data up to bin 17 were analyzed in this study, to avoid the use of spurious data from the bottom. All recorded data were used to investigate the structure and variability of the physical parameters but also to explain their relationships in time and frequency domains. Surface salinity and surface temperature data were measured at 0.5 m from the free surface of the ocean. Surface current was obtained by averaging the ADCP readings in the upper three bins (depth varying from 1.5 to 3.5 m). Initially, those data with values well above and below the threshold criteria (± 3 standard deviation) were eliminated. Most of the gaps were unitary and evenly distributed over the time series. Linear interpolation was used to replace missing data. The main gap occurred between December 9 and 12, 2016, with 53 hours of extension (representing 0.68% of total time series). The maximum gap found in ADCP measurements represents 3.6% of total time series for current velocity and direction.

Wind and current vectors were decomposed into longitudinal (y) and transverse (x) components, using a 37° clockwise axis rotation from true north, making the y-component parallel to the coast (alongshore component) and x-component perpendicular to the coast (cross-shore component). Alongshore and cross-shore wind stress were calculated using the classical formulation, with wind velocities measured at 10 m height. Since the anemometer is placed at 3.3 m above sea level, we assumed a logarithm wind profile (Panofsky and Dutton, 1984) to compute the wind components at 10 m. Positive (negative) values for both alongshore surface currents and wind stress indicate northeastward (southwestward) flow. Positive (negative) values for both cross-shore surface currents and wind stress indicate southeastward (northwestward) flow.

Basic statistics were calculated for all hydrological, oceanic, and atmospheric parameters.

A full tidal harmonic analysis was performed applying the methodology of Pawlowicz et al. (2002) using the mean profile of the detrended zonal (u or eastward) and meridional (v or northward) components of the current. The T_Tide toolbox was performed using the complex variable (u + iv) to characterize the tidal ellipses. The tidally driven

currents were reconstructed based on the harmonic constituents and subtracted from the detrended zonal and meridional components of the current. The resulted currents had their axes rotated in 37° clockwise from true north to obtain the along- and cross-shore components, which were used to study the structure and variability of currents and their relationship with other properties. Only constituents whose signal to noise ratios (SNR) are greater than 5 were considered as significant in this work. We used the original (not filtered) data of both mean zonal and meridional currents in the tidal analysis.

Trends were removed from each time series. A Lanczos-squared low pass filter was used to remove periods shorter than 40 h, while the high-frequency variations were obtained by removing the estimated low-frequency data from the original (not filtered) recorded data. Spectral analysis was made using low and high-frequency data to identify periods of high-energy events in the time series. The spectral analysis was based on Welch (1967), using a Hanning type window applied over 1/8 of the series total length with 50% overlap. Therefore, the average of spectral power density was estimated over 15 segments of the time series.

Cross-correlation analysis was used to investigate the relationships between detided surface currents and wind stress with original, low- and high-frequency data.

Daily freshwater discharges of the river systems Camaquã and Jacuí-Taquari were calculated with the rating curve method (Jaccon and Cudo, 1989) using values of water level measured by the National Department of Waters and Electrical Energy (DNAEE). The sum of daily discharges of Jacuí, Taquari, and Camaquã rivers was employed (Marques, 2005), while the hourly surface salinity, wind stress, and surface currents were converted into daily averages prior to the analysis. Initially, wavelet analysis was used to investigate the main cycles of Patos Lagoon's outflow (Torrence and Compo, 1998). Then, lagged cross-correlations were calculated between daily river discharge and daily averages of surface salinity, alongshore and cross-shore components of wind stress and surface currents.

Stationarity tests were applied to each time series (Thomson and Emery, 2014). The probability density function of each time series was found

time-dependent; thus, all the oceanic and atmospheric time series were considered non-stationary. Hence, the main cycles and the changes in the seasonal pattern were also studied using wavelet analysis with an adaptation of the Morlet wavelet method, as described by Torrence and Compo (1998).

To illustrate how wind stress and surface currents act over Patos Lagoon's plume, we examined the plume's behavior during the passages of five frontal systems between June to mid-August 2017 using true color composition of MODIS-Aqua Level 1B images, with 500 m resolution, obtained from <https://www.usgs.gov>. The cloud-free images were obtained before and during (or immediately after) the passage of each meteorological event. The five frontal systems (F1 to F5) crossed the study area in the following periods: June 08 to 13, 2017 (F1); June 17 to 21, 2017 (F2); June 29 to July 02, 2017 (F3); July 15 to 22, 2017 (F4); and August 08 to 10, 2017 (F5). During this approximately 2.5-month period, the hourly winds, surface salinity, and surface currents were investigated.

RESULTS AND DISCUSSION

This section is organized as follows: at first, a brief statistical description is provided regarding winds, river discharge, and oceanographic properties; secondly, current structure and variability are examined, followed by tidal analysis of mean current profile. Then, an emphasis is given to surface current variability and its relationship with winds and river discharge, with special focus on the winter period when cold frontal systems crossed the study area.

DESCRIPTION OF WINDS, RIVER DISCHARGE, AND OCEANOGRAPHIC PROPERTIES

Figure 2 shows the 325 days of continuous observations on original wind stress (Figures 2A and 2B), alongshore and cross-shore currents (Figures 2C and 2D), surface salinity (Figure 2E), and surface temperature (Figure 2F) records. Only surface currents (mean of bins 1 to 3, varying from 1.5 m to 4.5 m) were used.

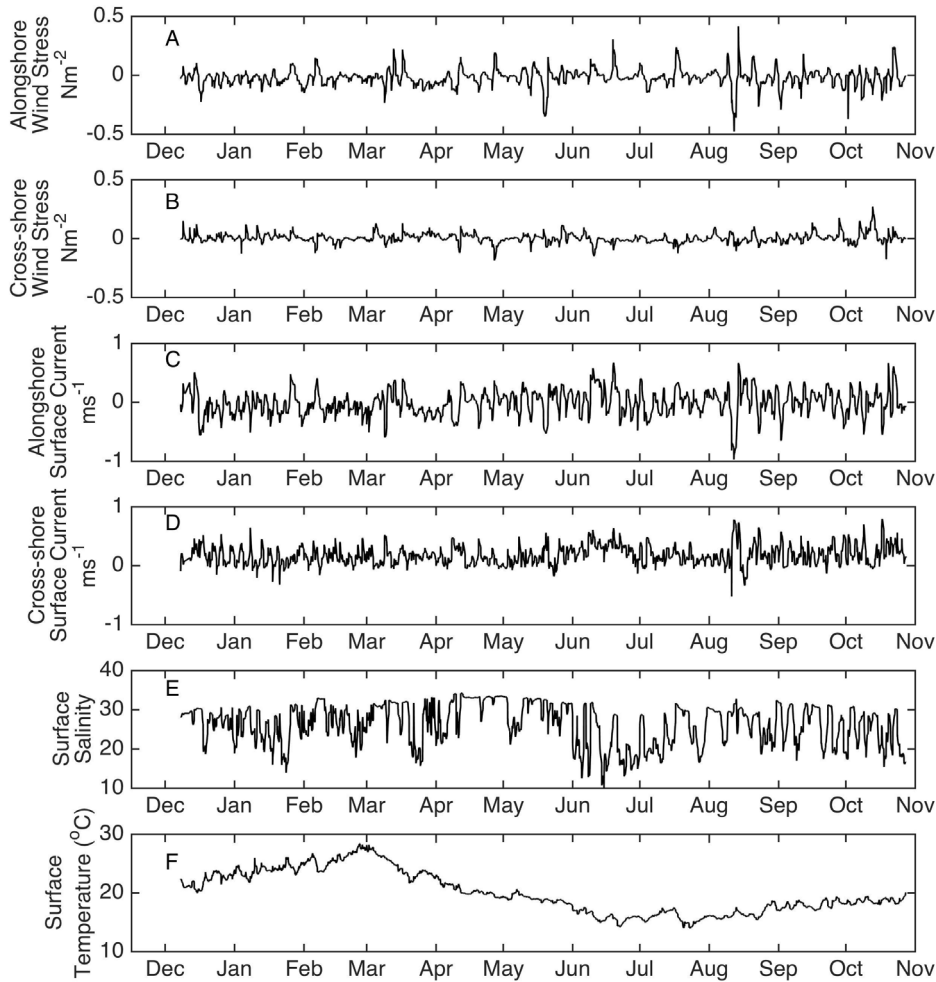


Figure 2. Hourly time series of: (A) alongshore wind stress; (B) cross-shore wind stress; (C) alongshore surface current; (D) cross-shore surface current; (E) surface salinity and (F) surface temperature.

The daily freshwater discharges of the river systems Camaquã and Jacuí-Taquari, and the mean daily salinity measured at buoy RS05 (Figure 3), also presented certain variability within the studied period. The mean daily average discharge over the period was $1984.3 \text{ m}^3 \text{ s}^{-1}$, with a standard deviation of $1794.0 \text{ m}^3 \text{ s}^{-1}$. The maximum (minimum) daily discharge happened in July (May) with a river discharge of 9345.5 (491.0) $\text{m}^3 \text{ s}^{-1}$ (Figure 3). The lagged cross-correlation between daily river discharge and daily salinity was -0.41 ($p < 0.05$), indicating that river discharge lead

salinity for 11 days. Notably, the minimum salinity (Figure 3) was reached in mid-June, after the maximum river discharge, which occurred at the beginning of June.

The wind rose diagram (Figure 4A) exhibits the well-known prevalence of northwest winds, with the incursion of southwestern winds due to cold frontal systems, while the surface current rose diagram (Figure 4B) shows the dominance of southeastern/eastern velocity at the inner shelf, as exposed and discussed in previous studies (Pereira, 1989; Zavialov et al., 2002; Marques et al., 2009).

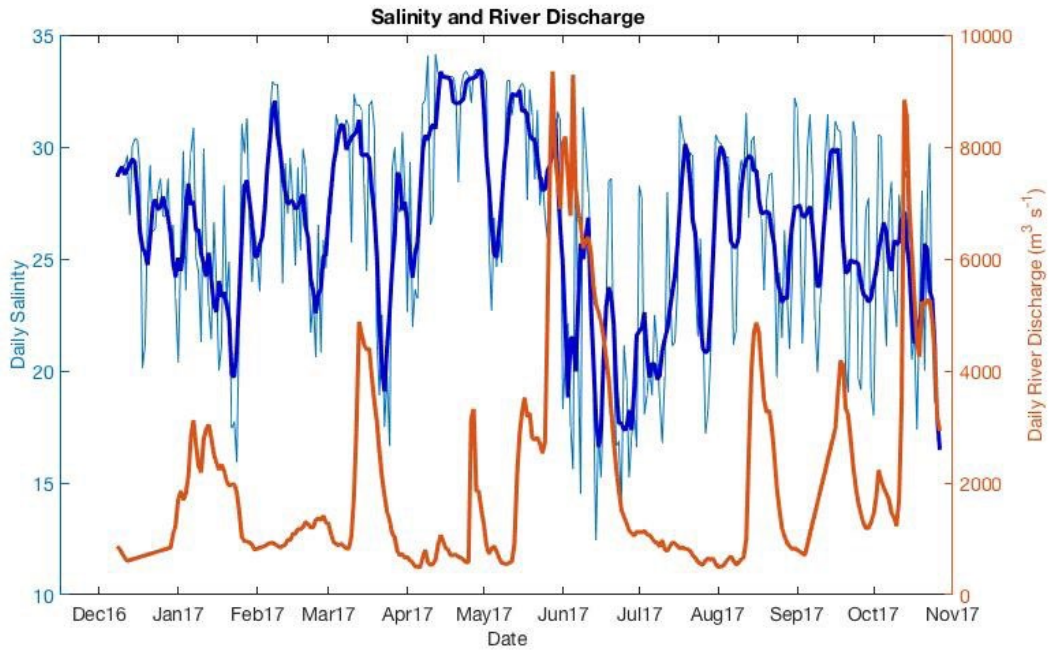


Figure 3. Time series of daily river discharge (red line) and daily salinity (light blue line) at buoy RS05 from December 8, 2016, to October 27, 2017. The thick blue color is a moving average filter with a 5-day span to smooth the daily salinity data. The daily salinity was calculated from 0 to 23 h.

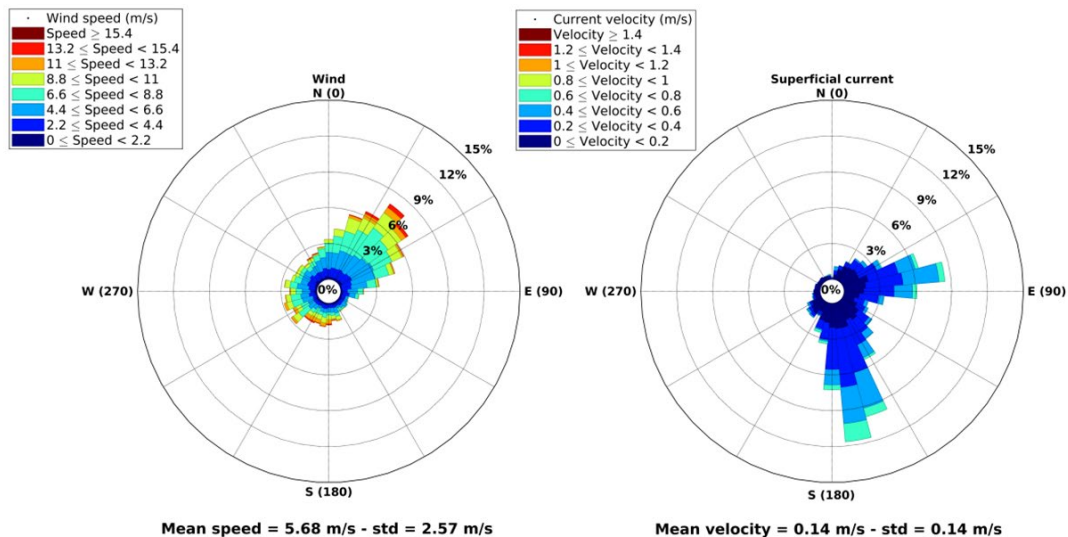


Figure 4. The (A) wind and (B) surface current rose diagrams. For winds, direction indicates where the wind blows from. For currents, direction indicates where currents flow to.

Table 1 presents the basic statistics for the metocean properties measured by the moored buoy. The averaged properties over depth and time of each time series suggests negative (southward) alongshore velocity flow of about

-0.006 m s^{-1} , with negative alongshore wind stress (southward) of about -0.023 N m^{-2} . The measured data supports the once popular conception of the mean southward flow of tropical origin over the inner shelf.

Table 1. Basic statistics for alongshore and cross-shore wind stress, alongshore and cross-shore surface currents, temperature, and salinity for all the time series. Positive (negative) values for both alongshore surface currents and wind stress indicate northeastward (southwestward) flow. Positive (negative) values for both cross-shore surface currents and wind stress indicate southeastward (northwestward) flow.

Property	Mean	Standard Deviation	Minimum	Maximum
Alongshore wind stress (N m^{-2})	-0.023	0.104	-0.426	0.427
Cross-shore wind stress (N m^{-2})	0.007	0.060	-0.320	0.359
Surface alongshore current (m s^{-1})	-0.006	0.220	-0.704	0.666
Surface cross-shore current (m s^{-1})	0.157	0.170	-0.601	0.694
Salinity	26.218	5.318	10.610	34.570
Temperature ($^{\circ}\text{C}$)	20.103	3.619	13.410	29.600

On the other hand, a northward flow was reported in previous studies (Campos et al., 1996; Zavialov et al., 1998, 2002; Piola et al., 1999). Zavialov et al. (2002) is considered the first study with *in situ* data using two current meters, one at 15 and the other at 40 m depth in a mooring station ($32^{\circ}41'S-51^{\circ}27'W$), from March 4 to August 2, 1997. The authors reported a northward current at the Brazilian continental shelf, despite the negative wind stress (southward), using a 151 day long time series for a 15 m current analysis. The mooring station in Zavialov et al. (2002) is located at $32^{\circ}17.76'S$ and $52^{\circ}1.44'W$, 20 nm away from the SiMCosta RS05 mooring buoy. To investigate the northern flow occurrence reported by Zavialov et al. (2002) and identify possible similar patterns in the behavior of current between their time series and this study, a comparative investigation was made using a similar time period (March 4 to August 2, 2017). The mean depth over the entire series suggests positive (northward) alongshore velocity flow of approximately 1.3 cm s^{-1} with negative wind stress (southward) alongshore of about -0.014 N m^{-2} . For the time frame of March 4 to August 2, 2017, the results are similar to those found by Zavialov et al. (2002) and indicate a northern flow occurrence on the southern Brazilian continental inner shelf within that period.

SURFACE WATER MASS

We used both low-frequency (period >40 h) surface salinity and temperature to examine the temporal evolution of both properties. Figure 5 shows the Temperature-Salinity-Time diagram, in which we can observe that surface temperature and surface salinity varied from 13.99 to 28.25°C

and from 11.33 to 35.16 , respectively. The colored Temperature-Salinity (TS) dotted lines are mostly orientated along the horizontal axis (constant temperature), due to the intrusion of Patos Lagoon's plume. Once the plume spread offshore reaching the RS05 buoy, salinity decreases rapidly with a small change in temperature.

During wintertime, a combined outflow of La Plata estuary (situated approximately 36°S) and southerly winds develop a buoyant coastal plume (La Plata plume) that extends northward along the Uruguayan and southern Brazilian continental shelf (Piola et al., 2008). Depending on wind and discharge conditions, the La Plata plume can reach the southern Brazilian inner continental shelf around 32°S . When this happens, Patos Lagoon's plume is embedded into this low salinity plume derived from La Plata estuary (Burrage et al., 2008). A close examination of TS-time diagram shows thermohaline indices similar to La Plata's plume when Patos Lagoon's plume is away from the RS05 buoy location.

Piola et al. (2000) used historical hydrographic data to suggest that, in the austral winter, La Plata's plume reaches Cape Santa Marta Grande (28°S), while it retracts to 32°S in the summer. Numerical experiments conducted by Pimenta et al. (2005) have shown that under steady southwesterly winds around 8 m s^{-1} and La Plata flow of nearly $15,000 \text{ m}^3 \text{ s}^{-1}$, La Plata's plume extended northeastward, reaching 32°S (30°S) after approximately 5 (10) days. A close inspection on alongshore wind records (not shown) showed, after a short period (March 18 to April 6, 2017) of northeast winds, that several meteorological frontal systems crossed the southern Brazilian region. La Plata's outflow on June 6, 2017, was about

22,500 m³ s⁻¹ (O. Möller, personal communication) and southwesterly winds near 5 m s⁻¹. Afterwards, a successive meteorological frontal system with southwestern winds crossed the region, which certainly pushed the low salinity further up-coast. The inspection of several weekly MODIS (4 km resolution) of sea surface temperature images from April (Figure 6) to August 2017 (not shown) led us

to believe that La Plata's plume occupied most of the Brazilian inner shelf for most of the winter season and, therefore, Patos Lagoon's plume was embedded into this relatively low salinity plume derived from the La Plata estuary. In other periods of time, the Patos Lagoon's plume was embedded into Subtropical Shelf Water, a mix of La Plata water and Tropical Water (Möller et al., 2008).

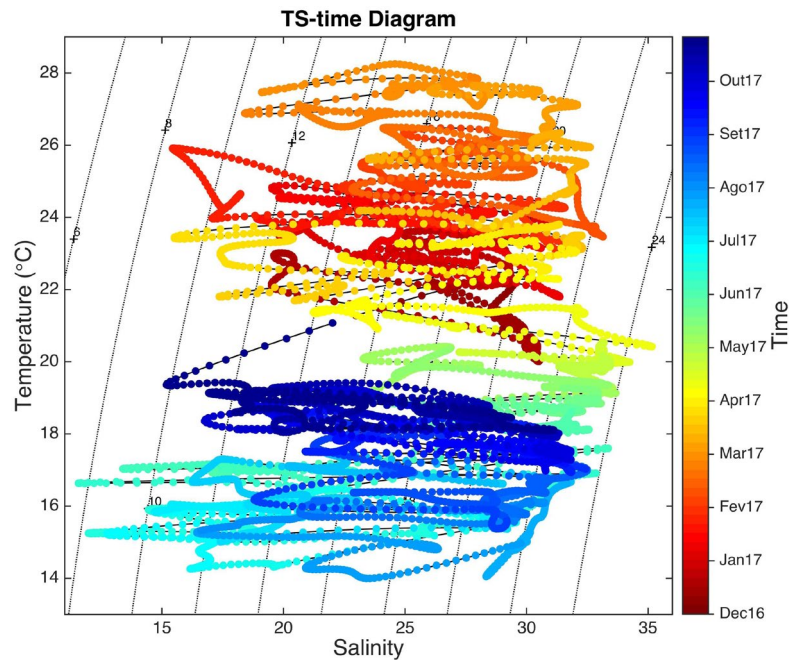


Figure 5. Temperature-Salinity-Time diagram.

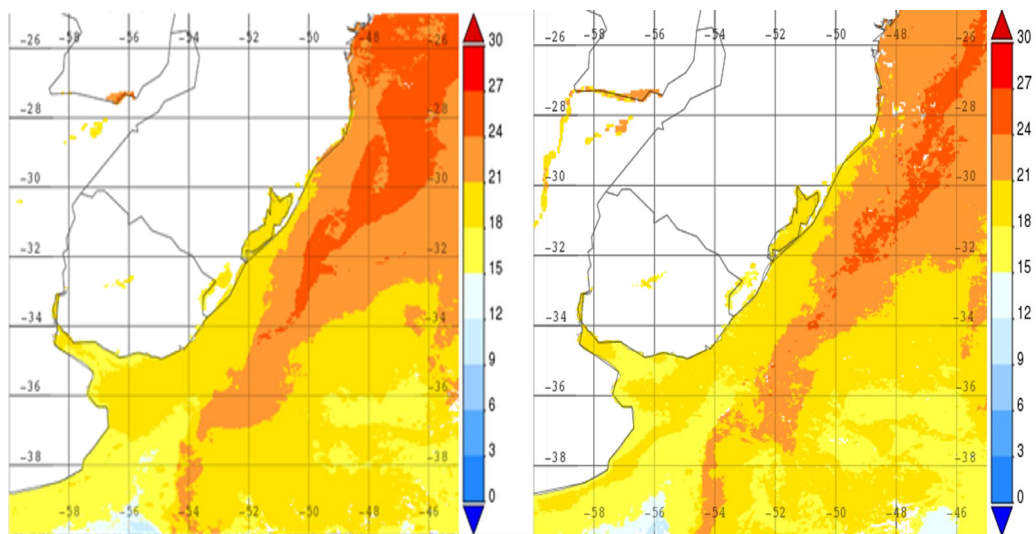


Figure 6. Weekly (8 days) MODIS SST images showing the La Plata incursion northwards along the southern Brazilian coast. Images are from April 6 to 14 (A) and April 22 to 30 (B), 2017. Source: Giovanni (NASA).

CURRENT STRUCTURE AND VARIABILITY

The vertical current structure and variability are discussed in this section using original (not filtered) and low-frequency filtered data. The RS05 buoy is placed at 20 m depth, but only depths between 1.5 m to 17.5 m were analyzed (bin 1 to bin 17) to avoid spurious data close to the ocean bottom. The vertical profile was analyzed using the along- and cross-shore components of currents. To understand the vertical profile structure, two approaches were chosen: (a) Hovmöller diagrams of alongshore and cross-shore currents as a function of time and depth. Low pass filtered data was used to improve visualization and analysis; (b) usage of the mean vertical profile to understand the main flow along with the profile (bins 1 to 17).

Figure 7 shows the vertical distribution of currents in alongshore (Figure 7A) and cross-shore (Figure 7B). Isoline zero represents changes in the flow's direction. It can be intuitively observed that both profiles are intermittent and vary quite often through time. The vertical distribution in the alongshore component exhibits a certain homogeneity with slightly larger (smaller) velocities in surface/intermediate (bottom) waters. The southern main flow seems predominant, especially from December to May, which has higher velocities in intermediated waters. From mid-June to October, southern flows are more intense and are associated with the typical seasonal cold front passages. Northern flows were predominant during mid-June.

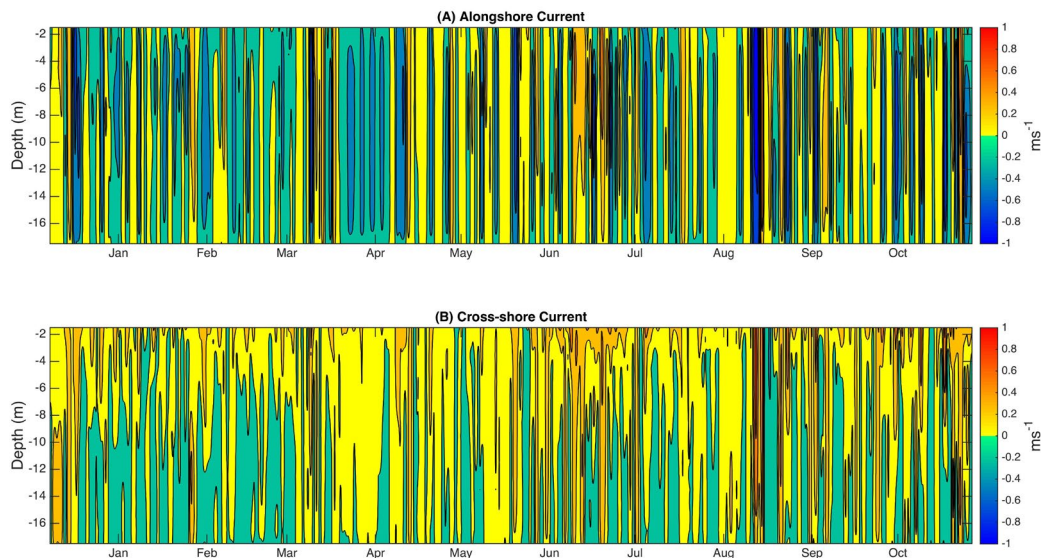


Figure 7. Vertical distribution of the alongshore (A) and cross-shore (B) currents. The components data were filtered using a Lanczos low-pass filter (periods > 40 h). The black contour lines represent zero values.

On the other hand, the cross-shore velocities behave differently than the alongshore. Overall, velocity variations were close to zero throughout time and, consequently, smaller. Differently from what is observed in alongshore velocities, in which velocities are similar along the profile, in cross-shore component, velocities exhibit sometimes the same flow orientation along with the profile. Although, mostly surface waters have different or opposite orientation comparing to intermediate and bottom velocities. In general, the first half of the vertical profile (1.5 m to 10.5 m depth) presents

eastern oriented velocities, while the second half (10.5 m to 17.5 m depth) exhibits a western orientation. This behavior is particularly visible during austral winter (June to September) and may be associated with river discharges. Zavalov et al. (2002) reported a drastic decay in currents during the austral winter, a time in which no significant reduction of wind forcing was evident. They hypothetically attributed this to the impact of a very stable salinity-controlled stratification that forms in a narrow subsurface layer due to enhanced river discharges from Patos-Mirim and

La Plata estuaries, effectively isolating deeper layers from the atmospheric forcing. A decrease in the monthly average salinity was found during Austral winter, which might be associated with cross-shore current behavior.

The mean vertical profiles for alongshore and cross-shore velocities in the entire time series (Figure 8) show southwestward and southeastward flow, respectively. The mean alongshore current in the water column is -3 cm s^{-1} for the entire period (Figure 8A). The overall southward-oriented current has been found in previous studies in the Brazilian southern inner shelf where the buoy is located (Palma et al., 2008; Costa and Möller, 2011).

The mean cross-shore current for the entire period (Figure 8B) has shown dominant positive (southeastward) values with larger velocities in surface waters. The mean cross-shore current in the water column is 7 cm s^{-1} for the entire period. The vertical distributions of alongshore and cross-shore currents were not uniform from surface to bottom. Wind and bed stresses change the mean current profile in the near-surface and bottom, respectively. Slightly higher velocities are found in intermediate depths. The mean cross-shore vertical profile is southeastward oriented with smaller velocities (close to zero) near the bottom. Continental discharges also contribute to the variability of surface currents in the locality.

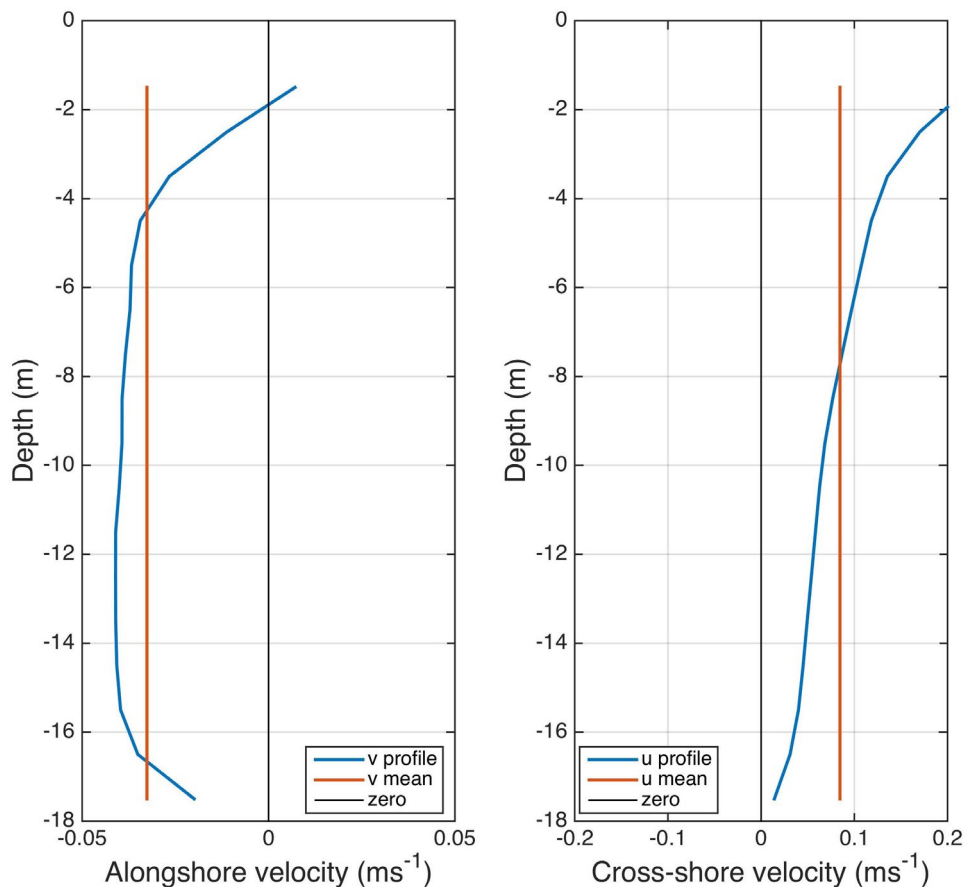


Figure 8. The mean vertical (A) alongshore and (B) cross-shore currents (blue lines) for the entire 325 days period. Positive (negative) alongshore currents are directed to the northeast (southwest) while positive (negative) cross-shore currents are southeastward (northwestward). The vertically averaged values are shown in red vertical lines.

ANALYSIS OF TIDAL CURRENTS

Table 2 shows the tidal constituents and ellipse parameters. The diurnal tidal constituent O1 (major amplitude = 3.81 cm s^{-1}) is confirmed as dominant for the location, followed by M4 (1.82 cm s^{-1}), K1 (1.80 cm s^{-1}), and M2 (1.42 cm s^{-1}). The tidal current resulting from the combination of the ten main tidal constituents can explain only 1.7% of the total variance of current, a clear indication that tides play a negligible role in the local current variability. Similar results were found in previous works (Moller et al., 2001; Zavialov et al., 2002; Costa and Möller, 2011), in which tidal currents were seen as very weak and predominantly diurnal. Notably, the M4 amplitude (and energy) is higher than its parental M2 amplitude. Green et al. (2018), using Topex TPX09 data, found that the beat of the diurnal

spring-neap and the semi-diurnal spring-neap cycle is very close to the period of M4. Therefore, an increase in M4 amplitude is expected when a timed combination exists between M4 and both the diurnal neap and semi-diurnal spring cycle. Our results agree with Green et al. (2018).

The power density spectra of the original and detided currents data (Figure 9) for both zonal (Figure 9A) and meridional (Figure 9B) components have shown peaks associated with periods of diurnal (D), semi-diurnal (SD), quarter-diurnal (QD), and sixth-diurnal (D/6) tidal constituents. The diurnal harmonic is the most expressive followed by the quarter-diurnal and semi-diurnal, respectively. The detided current was calculated by subtracting the tidally driven currents from the original (not filtered) data.

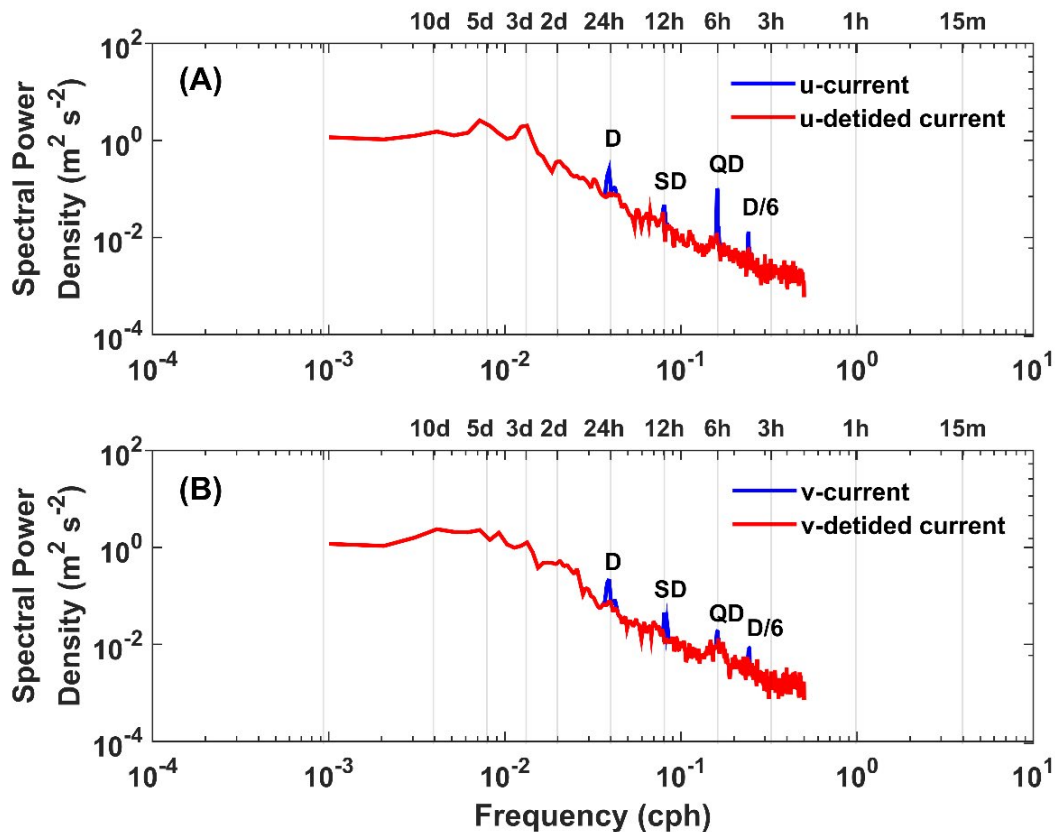


Figure 9. The spectral power density of the mean zonal (A) and mean meridional (B) components of currents. Original and detided mean currents are in blue and red lines, respectively. The diurnal (D), semi-diurnal (SD), quarter-diurnal (QD), and sixth-diurnal (D/6) frequencies are shown in the figure.

ANALYSIS OF SURFACE CURRENT VARIABILITY

This section is organized in three cases: 1) the structure and variability of surface currents (mean of bins 1 to 3, varying from 1.5 to 4.5 m) and their differences and similarities with wind stress, salinity, and temperature; 2) the impact of wind; and 3) the effect of river discharge on surface currents. We used only the detided along- and cross-shore surface currents in the analysis.

In cases 1 and 2, periods of high-energy events in the time series were identified through spectral analysis using low (period ≥ 40 h) and high (period ≤ 40 h) frequency filtered data. In case 3, high-energy events periods in the time series were identified through spectral analysis, as well as using original data. Finally, wavelet analysis was made using original (not filtered) data to investigate the main cycles and the changes in seasonal patterns of all the time series. Afterwards, wind stress and river discharge action on surface currents were further investigated with cross-correlation analysis using hourly data. The lagged cross-correlation was calculated between low-frequency (period ≥ 30 days) daily river discharge and daily averaged surface current.

To preserve the metocean signal variance under the spectral curve, we decided to use the variance-preserving form of the spectra for the wind stress, surface detided current, surface salinity, and surface temperature (Figure 10). Since the surface temperature presented a strong signal at low frequencies due to seasonal variation in solar radiation, we removed this seasonal signal from the time series. All the time series presented similar frequency patterns indicating the prevalence of high-energy events in common frequencies.

In the low-frequency band (period >40 h), periods of approximately 3 to 10 days for all the time series were common for both alongshore wind (Figure 10A) and currents (Figure 10C). The salinity preserving-variance spectrum (not shown) also presented a peak of around 3 to 11 days. The above time series presented common main peaks in 3 and 5.5 days.

On the other hand, no relevant energy was found in the low-frequency temperature (Figure 10F), cross-shore wind (Figure 10B), and surface cross-shore current (Figure 10D) spectra.

In the high-frequency band (period <24 h), the alongshore and cross-shore wind stress spectra have shown peaks at 24 h, which are associated with sea breeze (Figure 10A and 10B). The mean for both along- and cross-shore component spectra (Figure 10C and 10D) also presented a 24 h peak, however, the most energetic peak is associated with the mean for cross-shore current. The influence of wind as the main forcing mechanism acting on the local circulation was mentioned in previous studies (Castelao and Moller Jr, 2006; Möller et al., 2008; Marques et al., 2009, 2010). Since we are using detided currents, the existence of a 24 h energy peak, especially for the cross-shore component, suggests the existence of a daily forcing circulation associated to wind behavior.

The salinity preserving-variance spectrum (Figure 10E) shows high-energy events with periods of nearly 12 to 36 hours, with the main peak at 24 h as well, while the temperature spectrum (Figure 10F) shows high-energy events with periods at 12 and 24 h, which are related to daily variation of solar heating.

The results of the wavelet analysis using the data of detrended time series (not shown) indicates the importance of low-frequency processes and, once again, highlights that the most important events occurred in periods shorter than 8 days, except for the temperature time series. The main energetic peak occurred at approximately 5.5 days, coincident with the well-known passage of meteorological systems, which can vary from 3 to 17 days over the study region (Moller et al., 1996, 2001; Fernandes et al., 2001, 2002, 2004, 2005; Castelao and Moller Jr, 2006; Marques et al., 2010). The local energy spectrum of the alongshore wind stress shows maximum intensities between August to October and minimum between February and March. Similar patterns are found in surface currents and surface salinity.

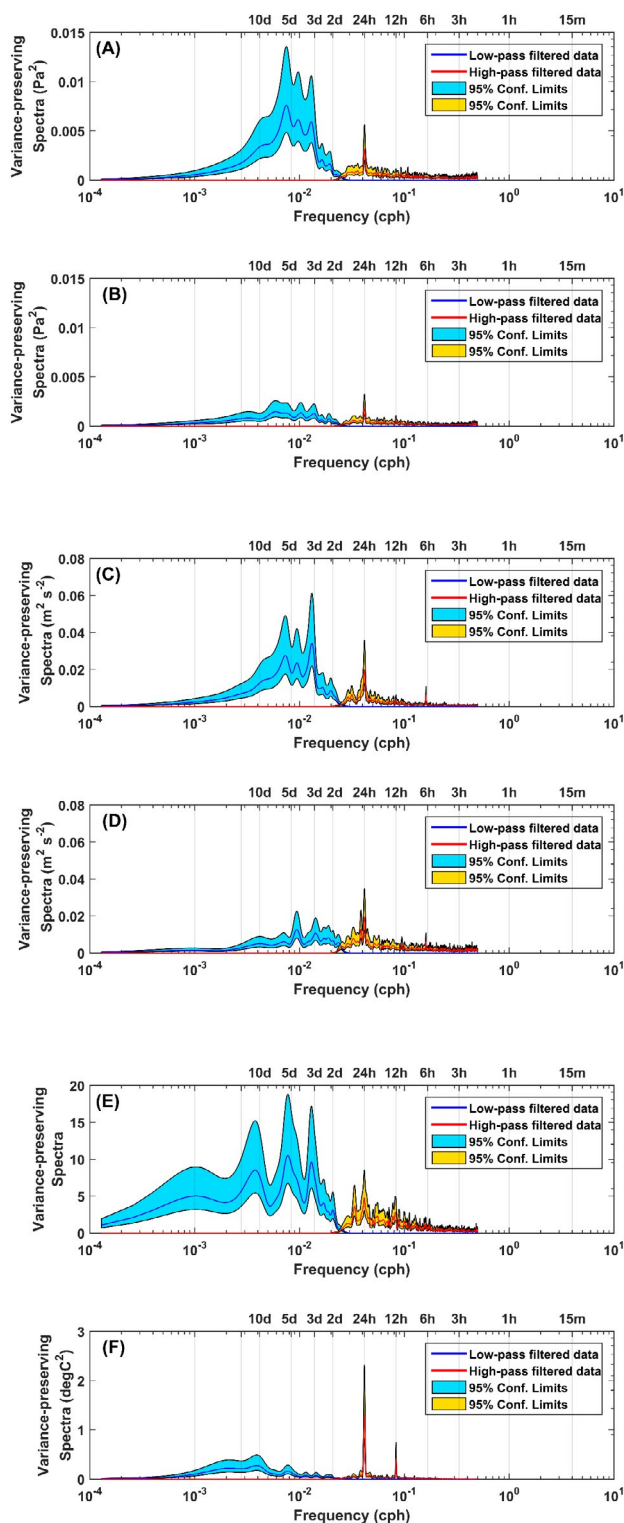


Figure 10. The variance-preserving spectra for the low (in blue) and high-frequency (in red) filtered data: (A) alongshore wind stress, (B) cross-shore wind stress, (C) alongshore detided surface current, (D) cross-shore detided surface current, (E) surface salinity, and (F) surface temperature (after removal of seasonal variation). Since the surface temperature presented a strong signal at low frequencies due to seasonal variation in solar radiation, we removed this seasonal signal from the time series.

WIND ACTION ON SURFACE CURRENTS

Wind stress impact on surface currents was further investigated with temporal cross-correlation between original, low- and high-filtered hourly data, in four different scenarios: 1) both alongshore wind and current; 2) both cross-shore wind and current; 3) alongshore wind and cross-shore current; and 4) cross-shore wind and alongshore current. The lagged cross-correlations between both alongshore wind and current have shown maximum positive correlation for original ($r=0.73$, $p<0.05$) at lag 3 h, low-frequency ($r=0.79$, $p<0.05$) at lag 5 h, and high-frequency filtered data (0.60 , $p<0.05$) at lag 3 h. On the other hand, weakly negative correlations between both cross-shore wind and current were found for original (-0.23 , $p<0.05$), low-frequency (-0.26 , $p<0.05$), and high-frequency (-0.17 , $p<0.05$). Alongshore (cross-shore) winds were even less correlated with cross-shore (alongshore) currents.

The results highlight the importance of alongshore wind in the local circulation with surface waters quickly responding to wind action. On the other hand, the cross-shore wind has little impact to the local circulation. Previous studies reported similar results (Zavialov et al., 2002; Marques et al., 2009). Consequently, surface circulation along the coastline is mostly driven by

the alongshore wind; whereas cross-shore surface circulation is partly driven by wind and may suffer the influence of other forcing elements, such as continental discharge. The results suggest that superficial waters circulation in the buoy site follows the standard pattern, in which the wind plays a relevant driving mechanism for surface currents and coastal plumes (Zavialov et al., 2002; Piola et al., 2005; Möller et al., 2008).

RIVER DISCHARGE EFFECTS ON OCEANIC PROPERTIES

The global spectrum of river discharges indicates that most of the energy is located at low frequencies (period >14 days), with the main energetic peak around 34 days (Figure 11). The 16-day peak (Figure 11) seems to be associated with freshets due to meteorological frontal rainfalls (Moller et al., 2001). The local energy spectrum shows two main events – from May to June and August to September – associated with low discharge events occurring between 16- and 32-day period (Figure 13). A subtle cycle (not included as being greater than 95% confidence for a red noise process and, therefore, it was not delimited by thick contour line) is visible from June to August at the main energetic peak of 34 days period, especially from May to September.

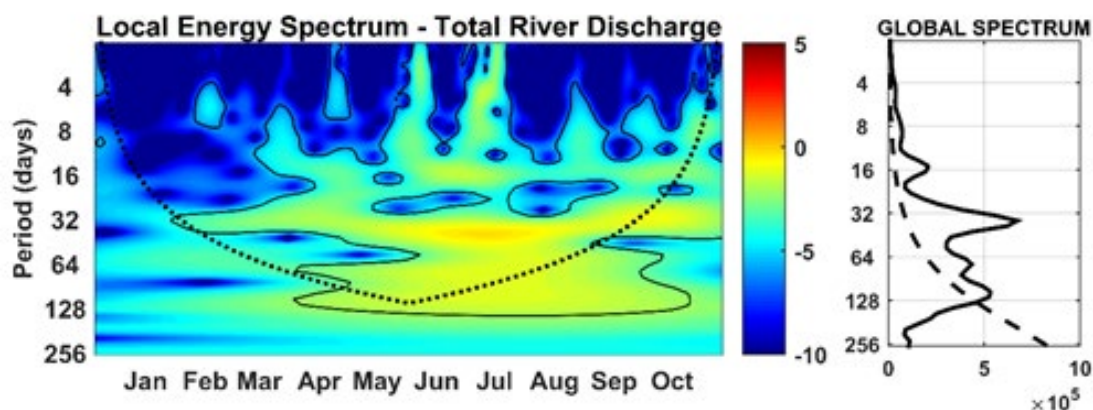


Figure 11. The local wavelet power spectrum of original (not filtered) daily river discharge time series using Morlet wavelet. Thick contour lines enclose regions with greater than 95% confidence for a red noise process with a lag 1 coefficient of 0.25. Cross-hatched regions indicate the cone of influence where edge effects become important. To the right of the local spectrum, the global wavelet power spectrum of the time series in which the dotted lines indicate the 95% confidence level.

Regarding the relationship between total river discharge and salinity, a negative correlation is expected based on the proximity of the buoy site to the mouth of Patos Lagoon since higher discharges imply greater flows towards the sea and, consequently, lower salinities at the buoy site. A negative lagged correlation ($r=-0.41$, $p<0.05$) was found between daily river discharge and daily salinity records, with discharge leading salinity for 11 days. A good lagged cross-correlation ($r=0.68$, $p<0.05$) between river flow and sea level at Rio Grande tide station was found using data from Dec 1, 2016, to Nov 30, 2017, with a lag of 10 days (O. Möller, personal communication). Since freshwaters from Jacuí, Taquari, and Camaquã rivers have to flow along the Patos Lagoon to reach the buoy position, a temporal delay exists in records of river discharges and salinity at buoy RS05. Those results suggest that freshwater flows, measured at the three main tributaries, took 10 days to reach the tide station and an extra day to reach the RS05 buoy.

However, salinity variation can be influenced by other factors as well, such as advection of water masses, tides, evaporation, precipitation, and wind-driven advection and mixing (Whitney, 2010). The La Plata plume can propagate northwards depending on wind and discharge conditions (Piola et al., 2005; Pimenta et al., 2005) lowering salinity records at the RS05 position in a certain period of the year. Tidal effects are minimal in the region. Evaporation and precipitation can also be negligible compared to the very dynamic process caused by wind that might play an important role on the behavior of Patos Lagoon's plume, and therefore, on the high-frequency salinity data.

For instance, previous studies (Malaval, 1922; Motta, 1969; Moller et al., 2001) reported that Patos Lagoon's discharges respond to wind forcing in a way that northeast winds contribute to the "emptying" of the lagoon, producing a seaward flow, while southerly winds, mainly those from southwestern, produce the opposite effect. These effects of wind on the outflow of Patos Lagoon occur at a temporal scale of hours (Moller et al., 2001), which can be undetected within the daily mean river discharge. The results indicated that river discharge acts as an important factor in salinity

variations at RS05 buoy's position since lower (higher) surface salinity records were associated with fresh (oceanic) waters. Wind forcing also plays a significant impact on salinity records at RS05 buoy, which will be further examined in the next section.

VARIABILITY OF SALINITY AND CURRENTS DURING THE PASSAGES OF COLD FRONTAL SYSTEMS

The results of the spectral and wavelet analysis indicate that winds are the main physical forcing mechanism acting on oceanic property variability. The dominance of north quadrant winds over the study region contributes to the prevailing southwestward migration pattern of the plume, while the passage of frontal systems over the area tends to transport the brackish waters to the north of Patos Lagoon's mouth. The time scale of this spreading is less than 1 day (Marques et al., 2010).

Figure 12 shows the time series of surface salinity (Figure 12A), alongshore and cross-shore wind stress (Figures 12B and 12C, respectively), alongshore and cross-shore surface currents (Figure 12D and 12E, respectively). The periods of the 5 cold front passages are highlighted (Figure 12).

Overall northeasterly winds prevailed before all 5 cold front passages. The beginning of the 5 frontal passages was characterized by southerly winds which resulted in currents towards the northeast. Salinity values were low before the frontal passages since RS05 was immersed in Patos Lagoon's plume (Figures 13A and 13C). For instance, before the first front passage, Patos Lagoon's plume was southwestward oriented (Figure 13A). During its passage, wind stress and surface current turned northeastward (Figure 12B and 12D), with an increase in salinity (Figure 12A) due to the displacement of brackish waters towards the northeast (Figure 13B) in agreement with da Silva et al. (2022). Similar behavior of winds, current, and plume displacement occurred during the passage of Front 2 (Figure 13C and 13D). Marques et al. (2009) have also shown that north quadrant winds induce upward velocities along the coast and enhance the advection of Patos Lagoon's plume southwestward with an increase of the stratification along the adjacent coastal region.

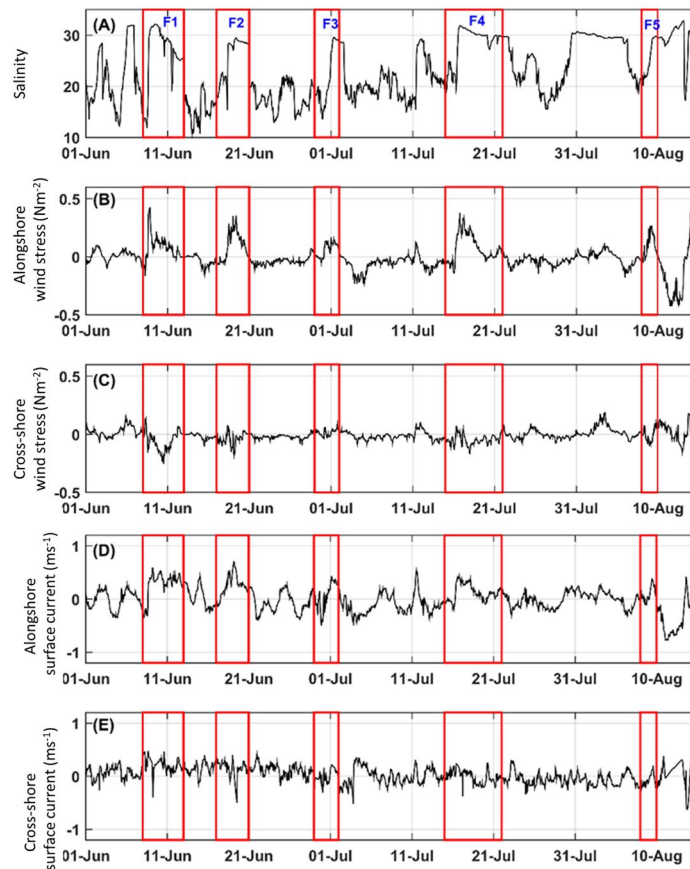


Figure 12. Time series of: (A) surface salinity; (B) alongshore wind stress; (C) cross-shore wind stress; (D) alongshore surface current; and (E) cross-shore surface current. Fronts 1 to 5 are highlighted by red squares.

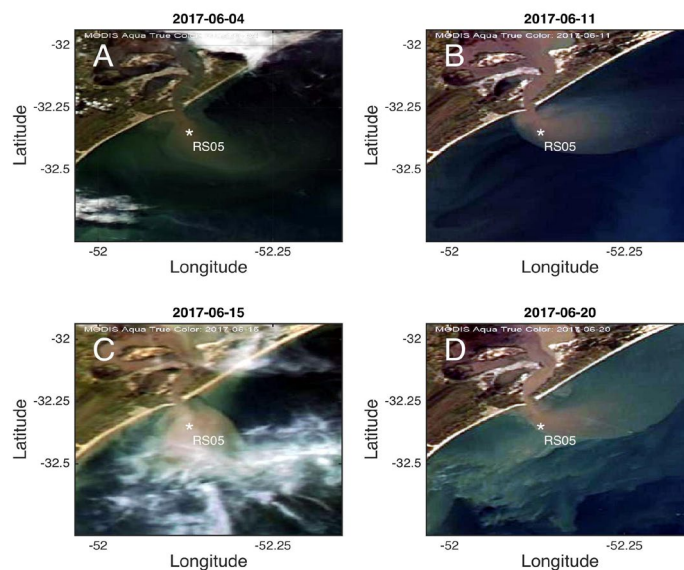


Figure 13. True color AQUA/MODIS images before (A) and during (B) Front 1 passage (right) and before (C) and during (D) Front 2 passage. Duration of Front 1: 2017-06-08 to 2017-06-13. Duration of Front 2: 2017-06-17 to 2017-06-21. The acquisition date of each image is also shown. The cloud-free images were obtained before and during (or just after) the passage of each meteorological event.

Northeasterly winds were also predominantly present before the passage of Fronts 3, 4, and 5 (Figure 12B), with surface currents flowing towards the northwest (Figure 12D) and a southwestward-oriented plume (Figures 14A, 14C and 14E) in agreement with Marques et. al. (2009) and da Silva et al. (2022). During the passage of frontal systems 3 and 4 (Figures 14B and 14D), winds started to blow from southwest, currents changed to northeast, and the plume spread northeast. In the case of cold front 5, Patos Lagoon's plume was attached to the coastline at the end of the front's passage (Figure 14F).

Surface and mean alongshore current are highly correlated ($r=0.79$ in both cases, $p<0.05$) with alongshore winds, with 1 h and 3 h delays, respectively. This is expected since it takes longer

for the entire water column to be influenced by wind stress. Surface salinity correlates with surface alongshore current ($r=0.51$, $p<0.05$) at lag 6 h and mean alongshore current ($r=0.50$, $p<0.05$) at lag 7 h. This relatively high time interval indicates that the RS05 buoy was completely immersed in the Lagoa dos Patos' plume (Figures 13A, 13C, 14A, 14C and 14E) and that a certain interval of time ($\sim 6-7$ h) was necessary for the entire plume to be displaced northward, which left the RS05 buoy immersed in La Plata's plume waters. Consequently, the oscillating behavior of salinity (see TS-time diagram, Figure 5), reaching low and high values in a relatively shorter interval of time, is associated with the presence/absence of Patos Lagoon's plume over the position of RS05, with the displacement of the plume being caused by southerly wind stress.

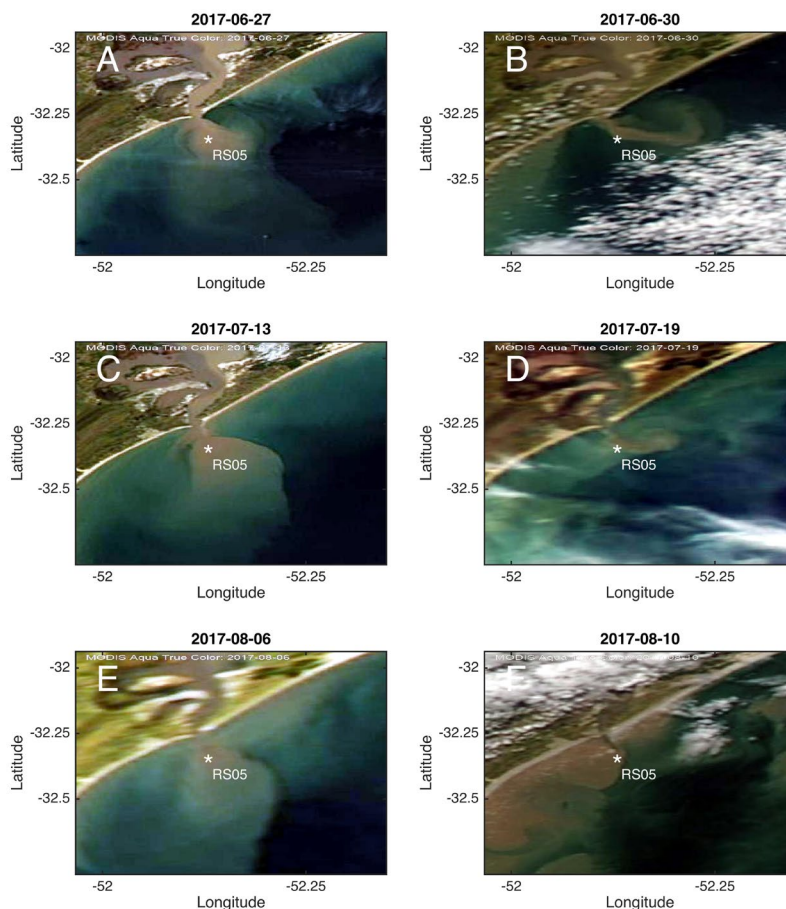


Figure 14. True color AQUA/MODIS images before (A, C, and E) and during (B, D, and C) frontal system passages. Patos Lagoon's plume is attached to the shore (F) at the end of the Front 5 passage. The duration of F3: 2017-06-29 to 2017-07-02; Duration of F4: 2017-07-15 to 2017-07-22; Duration of F5: 2017-08-08 to 2017-08-10. The acquisition date of each image is also shown. The cloud-free images were obtained before and during (or soon after) the passage of each meteorological event.

CONCLUSION

Metocean data, collected during 325 days by several instruments installed on a moored buoy, were used to study the vertical structure and variability of currents in the southern Brazilian inner shelf. The vertical distribution of the temporally averaged alongshore current was not uniform from the surface to the bottom, with slightly higher velocities in intermediate waters than in surface and bottom waters. The mean vertical alongshore and cross-shore current are southwestward and southeastward oriented with velocities of 3 and 7 cm s⁻¹, respectively.

The diurnal O1 tidal constituent is the major tidal constituent in both zonal and meridional components of the mean current profile, while the M4 harmonic presented the second most expressive amplitude in the zonal current component and mean current profile. Nevertheless, the tidal signal is negligible in the study area and represents approximately 1.7% of the variance of currents in the locality.

In the low-frequency band (period >40 h), alongshore wind stress, alongshore surface current, and surface salinity time series presented similar frequency patterns indicating the prevalence of high-energy events in periods of approximately 3 to 10 days, with a major peak around 5.5 days. In the high-frequency band (period <40h), cross-shore wind stress, cross-shore surface current, and surface temperature presented similar frequency patterns with a prevalence of high-energy events in periods of nearly 24 h. After the removal of seasonal solar heating, the temperature exhibits high-energy events in high-frequency (12 and 24 h) due to daily solar heating.

A high positive correlation between wind stress and surface currents was found only for both alongshore wind and current, whereas cross-shore winds were weakly correlated with surface currents. A lag of approximately 3h was found between both alongshore surface current and wind. The alongshore surface current was mostly driven by the alongshore wind while its cross-shore component was also driven by other mechanisms, such as continental discharge. The cross-shore wind seems to have insignificant participation to both along- and cross-shore surface current circulation.

The cycles of river discharge showed dominant signal at low frequency, with the main energetic peak at 34 days. Two main events – from May to June and August to September 2017 – associated with low river discharge events occurred between 16- and 32-days period. Patos Lagoon's outflow is responsible for variations in low-frequency surface salinity, as lower (higher) surface salinity records are associated with fresh (oceanic) waters.

The wavelet analysis for the metocean time series has shown that high-energy events for the alongshore wind stress are more common from August to October and not very often from February to March, with similar surface currents and salinity patterns.

Northeastern winds and southwestward-oriented plumes were a common pattern before the passage of cold frontal systems in the study region. The entrance of the frontal system with southwestern winds changed the current's orientation to northeast. An increase in surface salinity was observed during the frontal passages, which is a clear indication that salinity variations at the buoy site were mainly steered by the behavior of Patos Lagoon's coastal plume in time scales of hours.

ACKNOWLEDGMENTS

This research is partly funded by the Brazilian Coastal Monitoring System (SiMCosta) and Coordenação de Aperfeiçoamento de Pessoal de Nível Superior (CAPES, grant No. 2040/2017). The authors thank to Conselho Nacional de Desenvolvimento Científico e Tecnológico (CNPq) for grants No. 132603/2018-7 (JGS) and 311943/2015-2 (CAEG). Comments from Prof. Dr. O. O. Möller on earlier drafts of the manuscript are gratefully acknowledged. We appreciate all the valuable comments and suggestions of two anonymous reviewers, which helped us to improve the quality of the manuscript.

AUTHOR CONTRIBUTIONS:

J.G.S.: Investigation; Methodology; Software; Formal Analysis; Writing – original draft.

C.A.E.G.: Conceptualization, Supervision; Resources; Project Administration; Funding Acquisition; Writing – review & editing.

REFERENCES

- Beardsley, R. C. & Hart, J. 1978. A simple theoretical model for the flow of an estuary onto a continental shelf. *Journal of Geophysical Research*, 83(C2), 873. DOI: <https://doi.org/10.1029/jc083ic02p00873>
- Burrage, D., Wesson, J., Martinez, C., Pérez, T., Möller, O. & Piola, A. 2008. Patos Lagoon outflow within the Río de la Plata plume using an airborne salinity mapper: Observing an embedded plume. *Continental Shelf Research*, 28(13), 1625–1638. DOI: <https://doi.org/10.1016/j.csr.2007.02.014>
- Campos, E. J. D., Lorenzetti, J. A., Stevenson, M. R. & Stech, J. L. 1996. Penetration of waters from the Brazil–Malvinas Confluence region along the South American continental shelf up to 23°S. *Anais Da Academia Brasileira de Ciências*, 68(supl. 1), 49–58.
- Castelao, R. M. & Moller Jr, O. O. 2006. A modeling study of Patos lagoon (Brazil) flow response to idealized wind and river discharge: dynamical analysis. *Brazilian Journal of Oceanography*, 54(1), 1–17. DOI: <https://doi.org/10.1590/s1679-87592006000100001>
- Castro, B. M. de, Brandini, F. P. & Pires-Vanin, A. M. S. 2006. The Global Coastal Ocean: Interdisciplinary Regional Studies and Syntheses: The Sea. (Vol. 14, pp. 259–293). Cambridge: Harvard University Press.
- Castro, B. M. & Lee, T. N. 1995. Wind-forced sea level variability on the southeast Brazilian shelf. *Journal of Geophysical Research*, 100(C8), 16045–16056. DOI: <https://doi.org/10.1029/95jc01499>
- Castro, B. M. & Miranda, L. B. 1998. Physical Oceanography of the western Atlantic continental shelf between 41N and 34S. In: Brink, K. & Robinson, A. (Eds.). *The Sea: The Global Coastal Ocean* (Vol. 10, pp. 209–251). New York: Wiley.
- Chao, S.-Y. 1988a. River-Forced Estuarine Plumes. *Journal of Physical Oceanography*, 18(1), 72–88.
- Chao, S.-Y. 1988b. Wind-Driven Motion of Estuarine Plumes. *Journal of Physical Oceanography*, 18(8), 1144–1166.
- Chao, S.-Y. & Boicourt, W. C. 1986. Onset of Estuarine Plumes. *Journal of Physical Oceanography*, 16(12), 2137–2149.
- Costa, R. L. & Möller, O. O. 2011. Estudo da estrutura e da variabilidade das correntes na área da plataforma interna ao largo de Rio Grande (RS, Brasil), no sudoeste do Atlântico Sul, durante a primavera-verão de 2006-2007. *Revista Da Gestão Costeira Integrada*, 11(3), 273–281.
- Fernandes, E. H., Dyer, K. R. & Niencheski, L. F. H. 2001. Calibration and Validation of the TELEMAC-2D Model to the Patos Lagoon (Brazil). *Journal of Coastal Research*, (34), 470–488.
- Fernandes, E. H. L., Dyer, K. R. & Moller, O. O. 2005. Spatial Gradients in the Flow of Southern Patos Lagoon. *Journal of Coastal Research*, 21(4), 759–769.
- Fernandes, E. H. L., Dyer, K. R., Moller, O. O. & Niencheski, L. F. H. 2002. The Patos Lagoon hydrodynamics during an El Niño event (1998). *Continental Shelf Research*, 22(11–13), 1699–1713. DOI: [https://doi.org/10.1016/s0278-4343\(02\)00033-x](https://doi.org/10.1016/s0278-4343(02)00033-x)
- Fernandes, E. H. L., Mariño-Tapia, I., Dyer, K. R. & Möller, O. O. 2004. The attenuation of tidal and subtidal oscillations in the Patos Lagoon estuary. *Ocean Dynamics*, 54(3–4), 348–359. DOI: <https://doi.org/10.1007/s10236-004-0090-y>
- Framiñan, M. B. & Brown, O. B. 1996. Study of the Río de la Plata turbidity front, Part 1: spatial and temporal distribution. *Continental Shelf Research*, 16(10), 1259–1282. DOI: [https://doi.org/10.1016/0278-4343\(95\)00071-2](https://doi.org/10.1016/0278-4343(95)00071-2)
- Garvine, R. W. 1984. Radial spreading of buoyant, surface plumes in coastal waters. *Journal of Geophysical Research*, 89(C2), 1989–1996. DOI: <https://doi.org/10.1029/jc089ic02p01989>
- Garvine, R. W. 1999. Penetration of Buoyant Coastal Discharge onto the Continental Shelf: A Numerical Model Experiment. *Journal of Physical Oceanography*, 29(8), 1892–1909.
- Green, J. A. M., Bowers, D. G. & Byrne, H. A. M. 2018. A mechanistic classification of double tides. *Ocean Science Discussions*. Copernicus GmbH. DOI: <https://doi.org/10.5194/os-2018-72>
- Guerrero, R. A., Acha, E. M., Framiñan, M. B. & Lasta, C. A. 1997. Physical oceanography of the Río de la Plata Estuary, Argentina. *Continental Shelf Research*, 17(7), 727–742. DOI: [https://doi.org/10.1016/s0278-4343\(96\)00061-1](https://doi.org/10.1016/s0278-4343(96)00061-1)
- Guo, X. & Valle-Levinson, A. 2007. Tidal effects on estuarine circulation and outflow plume in the Chesapeake Bay. *Continental Shelf Research*, 27(1), 20–42. DOI: <https://doi.org/10.1016/j.csr.2006.08.009>
- Ikeda, M. 1984. Coastal flows driven by a local density flux. *Journal of Geophysical Research*, 89(C5), 8008–8016. DOI: <https://doi.org/10.1029/jc089ic05p08008>
- Jaccon, G. & Cudo, K. J. 1989. *Curva-chave: análise e traçado* (techreport). Brasília, DF: Departamento Nacional de Águas e Energia Elétrica.
- Kirincich, A. R. & Hebert, D. 2005. The structure of the coastal density front at the outflow of Long Island Sound during spring 2002. *Continental Shelf Research*, 25(9), 1097–1114. DOI: <https://doi.org/10.1016/j.csr.2004.12.014>
- Lentz, S. J. 1995. Sensitivity of the inner-shelf circulation to the form of the eddy viscosity profile. *Journal of Physical Oceanography*, 25(1), 19–28.
- Malaval, M. B. 1922. *Travaux du port et de la barre de Rio Grande, Brésil*. Paris: Eyrolles Editeurs.
- Mann, K. H. & Lazier, J. R. N. 2005. *Dynamics of Marine Ecosystems* (3rd ed.). Hoboken: Wiley. DOI: <https://doi.org/10.1002/9781118687901>
- Marques, W. C. 2005. *Padrões de variabilidade temporal nas forçantes da circulação e seus efeitos na dinâmica da Lagoa dos Patos, Rio Grande do Sul, Brasil* (mathesis). Universidade Federal do Rio Grande, Rio Grande.
- Marques, W. C., Fernandes, E. H. L., Moraes, B. C., Möller, O. O. & Malcherek, A. 2010. Dynamics of the Patos Lagoon coastal plume and its contribution to the deposition pattern of the southern Brazilian inner shelf. *Journal of Geophysical Research: Oceans*, 115(C10). DOI: <https://doi.org/10.1029/2010jc006190>
- Marques, W. C., Fernandes, E. H., Monteiro, I. O. & Möller, O. O. 2009. Numerical modeling of the Patos Lagoon coastal plume, Brazil. *Continental Shelf Research*, 29(3), 556–571. DOI: <https://doi.org/10.1016/j.csr.2008.09.022>

- Matano, R. P., Palma, E. D. & Piola, A. R. 2010. The influence of the Brazil and Malvinas Currents on the Southwestern Atlantic Shelf circulation. *Ocean Science*, 6(4), 983–995. DOI: <https://doi.org/10.5194/os-6-983-2010>
- McClimans, T. A. 1988. Physical Processes in Estuaries. In: Dronkers, J. & Leussen, W. (eds.), *Physical Processes in Estuaries* (pp. 55–69). Berlin: Springer. DOI: https://doi.org/10.1007/978-3-642-73691-9_4
- Mendes, J. C. 1984. *Elementos de estratiografia*. T.A. Queiroz.
- Mendonça, L. F., Souza, R. B., Aseff, C. R. C., Pezzi, L. P., Möller, O. O. & Alves, R. C. M. 2017. Regional modeling of the water masses and circulation annual variability at the Southern Brazilian Continental Shelf. *Journal of Geophysical Research: Oceans*, 122(2), 1232–1253. DOI: <https://doi.org/10.1002/2016jc011780>
- Miranda, L. B. 1972. *Propriedades e variáveis físicas das águas da Plataforma continental do Rio Grande do Sul*. (phdthesis). Instituto Oceanográfico da Universidade de São Paulo, São Paulo.
- Miranda, L. B. & Castro, B. M. 1979. Aplicação do diagrama TS estatístico-volumétrico à análise das massas de água da plataforma continental do Rio Grande do Sul. *Boletim do Instituto Oceanográfico*. Instituto Oceanográfico.
- Mitchum, G. T. & Clarke, A. J. 1986. The Frictional Nearshore Response to Forcing by Synoptic Scale Winds. *Journal of Physical Oceanography*, 16(5), 934–946.
- Moller, O. O., Castaing, P., Salomon, J.-C. & Lazure, P. 2001. The Influence of Local and Non-Local Forcing Effects on the Subtidal Circulation of Patos Lagoon. *Estuaries*, 24(2), 297. DOI: <https://doi.org/10.2307/1352953>
- Moller, O. O., Lorenzenti, J. A., Stech, J. & Mata, M. M. 1996. The Patos Lagoon summertime circulation and dynamics. *Continental Shelf Research*, 16(3), 335–351. DOI: [https://doi.org/10.1016/0278-4343\(95\)00014-r](https://doi.org/10.1016/0278-4343(95)00014-r)
- Möller, O. O., Piola, A. R., Freitas, A. C. & Campos, E. J. D. 2008. The effects of river discharge and seasonal winds on the shelf off southeastern South America. *Continental Shelf Research*, 28(13), 1607–1624. DOI: <https://doi.org/10.1016/j.csr.2008.03.012>
- Motta, V. F. 1969. *Relatório diagnóstico sobre a melhoria e o aprofundamento do canal de acesso pela barra do Rio Grande*. (techreport). Porto Alegre: Instituto de Pesquisas Hidráulicas da Universidade Federal do Rio Grande do Sul.
- Palma, E. D., Matano, R. P. & Piola, A. R. 2008. A numerical study of the Southwestern Atlantic Shelf circulation: Stratified ocean response to local and offshore forcing. *Journal of Geophysical Research*, 113(C11). DOI: <https://doi.org/10.1029/2007jc004720>
- Pawlowicz, R., Beardsley, B. & Lentz, S. 2002. Classical tidal harmonic analysis including error estimates in MATLAB using T_TIDE. *Computers & Geosciences*, 28(8), 929–937. DOI: [https://doi.org/10.1016/s0098-3004\(02\)00013-4](https://doi.org/10.1016/s0098-3004(02)00013-4)
- Pereira, C. S. 1989. Seasonal variability in the coastal circulation on the Brazilian continental shelf (29°S–35°S). *Continental Shelf Research*, 9(3), 285–299.
- Pimenta, F. M., Campos, E. J. D., Miller, J. L. & Piola, A. R. 2005. A numerical study of the Plata River plume along the southeastern South American continental shelf. *Brazilian Journal of Oceanography*, 53(3–4), 129–146.
- Piola, A. R., Campos, E. J. D., Möller, O. O., Charo, M. & Martinez, C. 1999. Continental shelf water masses off eastern South America – 20° to 40° S. In: *Symposium on Global Change Studies* (pp. 9–12). Boston: American Meteorology Society.
- Piola, A. R., Campos, E. J. D., Möller, O. O., Charo, M. & Martinez, C. 2000. Subtropical Shelf Front off eastern South America. *Journal of Geophysical Research: Oceans*, 105(C3), 6565–6578. DOI: <https://doi.org/10.1029/1999jc000300>
- Piola, A. R., Matano, R. P., Palma, E. D., Möller Jr., O. O. & Campos, E. 2005. The influence of the Plata River discharge on the western South Atlantic shelf. *Geophysical Research Letters*, 32(1). DOI: <https://doi.org/10.1029/2004gl021638>
- Piola, A. R., Möller, O. O., Guerrero, R. A. & Campos, E. J. D. 2008. Variability of the subtropical shelf front off eastern South America: Winter 2003 and summer 2004. *Continental Shelf Research*, 28(13), 1639–1648. DOI: <https://doi.org/10.1016/j.csr.2008.03.013>
- Piola, A. R. & Rivas, A. 1997. El Mar Argentino e sus Recursos Pesqueros. In: Boschi, E. (ed.) (Vol. 1, pp. 119–132). Buenos Aires: Instituto Nacional de Investigación y Desarrollo Pesquero.
- Silva, D. V. da, Oleinik, P. H., Costi, J., Kirinus, E. de P., Marques, W. C. & Moller, O. O. 2022. Variability of the Spreading of the Patos Lagoon Plume Using Numerical Drifters. *Coasts*, 2(2), 51–69. DOI: <https://doi.org/10.3390/coasts2020004>
- Soares, I. D., Kourafalou, V. & Lee, T. N. 2007. Circulation on the western South Atlantic continental shelf: 1. Numerical process studies on buoyancy. *Journal of Geophysical Research*, 112(C4). DOI: <https://doi.org/10.1029/2006jc003618>
- Stevenson, M. R., Dias-Brito, D., Stech, J. L. & Kampel, M. 1998. How do cold water biota arrive in a tropical bay near Rio de Janeiro, Brazil? *Continental Shelf Research*, 18(13), 1595–1612. DOI: [https://doi.org/10.1016/s0278-4343\(98\)00029-6](https://doi.org/10.1016/s0278-4343(98)00029-6)
- Thomson, R. E. & Emery, W. J. 2014. *Data Analysis Methods in Physical Oceanography*. Elsevier. DOI: <https://doi.org/10.1016/c2010-0-66362-0>
- Torrence, C. & Compo, G. P. 1998. A Practical Guide to Wavelet Analysis. *Bulletin of the American Meteorological Society*, 79(1), 61–78.
- Yankovsky, A. E. & Chapman, D. C. 1997. A Simple Theory for the Fate of Buoyant Coastal Discharges. *Journal of Physical Oceanography*, 27(7), 1386–1401.
- Zavialov, P., Möller, O. & Campos, E. 2002. First direct measurements of currents on the continental shelf of Southern Brazil. *Continental Shelf Research*, 22(14), 1975–1986. DOI: [https://doi.org/10.1016/s0278-4343\(02\)00049-3](https://doi.org/10.1016/s0278-4343(02)00049-3)
- Zavialov, P. O., Ghisolfi, R. D. & Garcia, C. A. E. 1998. An inverse model for seasonal circulation in the Southern Brazilian shelf: near surface velocity from the heat budget. *Journal of Physical Oceanography*, 28(4), 545–562.